GAVIN PUBLISHERS

Archives of Environmental Sciences and Environmental Toxicology

OPEN ACCESS

Research Article

Tang Z, et al.

DOI: 10.29011/2688-948X.100125

Numerical Predictions of Ultralow Cycle Fatigue Damage of Fixed Steel Members

Zhanzhan Tang[1,2#], Linghao Kong[1], Hanyang Xue[1#*], Hanqing Zhuge[3]

[1]College of Civil Science and Engineering, Yangzhou University, China

[2]Institute of Theoretical and Applied Mechanics, Czech Academy of Sciences, Czech Republic

[3]College of Civil Engineering and Architecture, Zhejiang University of Science and Technology, China

[#]Authors Contributed Equally

[*]**Corresponding author:** Hanyang Xue, College of Civil Science and Engineering, Yangzhou University, Yangzhou 225127, China

Citation: Tang Z, Kong L, Xue H, Zhuge H (2020) Numerical Predictions of Ultralow Cycle Fatigue Damage of Fixed Steel Members. Arch Environ Sci Environ Toxicol 3: 126. DOI: 10.29011/2688-948X.100126

Received Date: 21 October 2020; **Accepted Date:** 28 October 2020; **Published Date:** 04 November 2020

Abstract

A steel member usually loses its seismic resistance due to either instability in the structural level or ultralow cycle fatigue in the material level. At present, predictions of the ultimate strength and ductility of steel members have been established, but these for predicting ultralow cycle fatigue damage at joints has not been determined. 23 steel members with pipe cross-sections and 22 members with rectangular cross-sections are designed in this paper, and their mechanical behaviors and failure modes under repeated seismic loads are analyzed. Effective methods to predict the ultralow cycle fatigue damage of these members are proposed, including the predictions for the welds, the heat-affected zones and the base metals. The results show that, for pipe-section steel members, if the axial compression ratio is larger than 0.2, or the slenderness ratio is larger than 0.06, or the diameter-to-thickness ratio exceeds 0.05, the structural instability failure occurs prior to the ultralow cycle fatigue failure. If the diameter-to-thickness ratio is less than 0.03, ultralow cycle fatigue failure occurs first. For rectangular-section steel members, if the width-to-thickness ratio of the flange is larger than 0.5, the instability failure controls the safety of the steel members. However, if the width-to-thickness ratio of flange plate is less than 0.5, the member would experience ultralow cycle fatigue failure rather than the instability failure. The proposed formulas can significantly save the computational cost and predict the failure modes of steel members accurately.

Keywords: Steel member; Ultralow cycle fatigue; Cyclic void growth model; Damage index; Seismic design

Steel members with a fixed boundary at their both ends are the most commonly used elements in a steel structure, such as the transverse braces in a steel bridge and the beams/columns in a building structure. These kinds of members usually connect with each other through welding. Seismic disasters in the past 20 years show that, steel members are prone to lose their bearing capacities due to instability or Ultralow Cycle Fatigue (ULCF) during a strong earthquake [1-5].

Evaluation of the bearing capacity or ductility of a steel member considering the effect of structural instability has been studied by many researchers. Zheng, et al. studied the ductility of thin-walled rectangular columns, including two kinds of cross sections with and without longitudinal stiffeners [4]. The empirical formulas for ductility evaluation were proposed by them. Kono, et al. proposed the prediction methods of ultimate deformation of the steel piers under repeated loads through conducting parametric analysis [5]. Ge, et al., Usami, et al. and Ge, et al. proposed some empirical formulas to assess the ultimate strength of steel bridge piers [6-8]. Usami, et al. studied the bearing capacity evaluation of some box-section members under the combined actions of axial and eccentric compressions [9]. Zhou, et al. investigate the mechanical performance of steel members under bending moments, and the influence of residual stress was taken into account in their study [10]. To prevent instable failure mode, some related specifications can be found in the current codes regarding to the design of a steel member, e.g. the Chinese specification stipulates the stability evaluation method of the steel members under compression or bending moments [11], and the slenderness ratio and width-to-thickness ratio of a steel member in bridges are also specified [12]. Moreover, the Japanese specification stipulates the formula to compute the ductility of steel bridge piers [13], and the AASHTO specification provides some suggestions for the seismic design of steel members [14]. On the other hand, the

prediction of ultra-low cycle fatigue of steel material based on microscopic damage mechanism has been the focus of scholars. Rice, et al. analyzed the growth of spherical void in an infinite ideal elastic-plastic continuous material, and proposed the Void Growth Model (VGM) [15]. Kanvinde, et al. proposed the Cyclic Void Growth Model (CVGM), which can be used to predict the crack initiation induced by ultralow cycle fatigue [16-19]. Liao, et al. and Yin, et al. calibrated the material parameters in the cyclic void growth model [20-22]. Zhou, et al. and Wang, et al. studied the ultralow cycle fatigue failure of steel structure joints through experiments, and verified the accuracy of the model [23-25]. Xie, et al. [26] studied the failure modes of a thin-walled steel arch bridge under strong earthquakes, and reported that ultralow cycle fatigue failure of a thin-walled steel member may occur prior to buckling. During a catastrophic earthquake, no matter which kind of the failure modes occur, the steel member will lose its bearing capacity [1,22]. Therefore, the relationship between these two failure modes should be clarified.

In order to study the failure modes of the fixed-end steel members under cyclic loads, a series of steel members are designed considering different parameters, such as the diameter-to-thickness ratio, the width-to-thickness ratio, the slenderness ratio and the axial compression ratio. The cyclic void growth model is compiled as a subroutine program and embedded into the finite element software for analysis. The evolution of ultralow cycle fatigue damage index of the steel members in the weld zone, the heat-affected zone and the base metals are discussed. The empirical formulas to predict the ultralow cycle fatigue damage index of the fixed-end steel members are proposed, which can effectively evaluate the failure modes and facilitate the structural seismic design of the steel members [27,28].

Design and Numerical Models of Steel Members

Design of the steel members

Figure 1 shows the steel members with fixed boundaries at their both ends, where pipe and rectangular cross-sections are adopted respectively, l is the length of the member, a is the diaphragm spacing, R is the radius of the pipe cross-section, t is the thickness of the steel plate, B and D are the width and depth of the rectangular cross-section, a' is the transverse spacing between each longitudinal stiffener, t_0 is the thickness of the longitudinal stiffener, an axial force N and a cyclic force H are applied to one of the ends of the members.

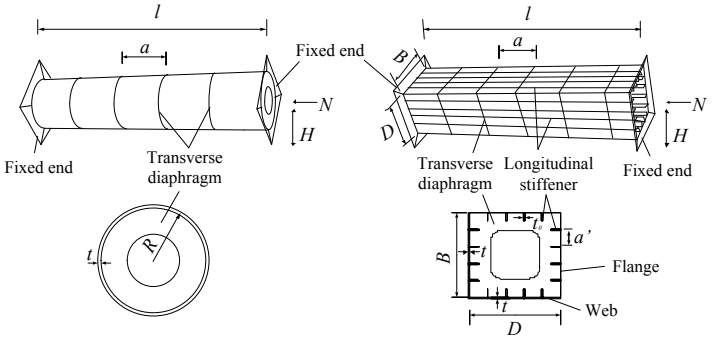

Figure 1: Structural design and cross-section of the member.

Some design parameters of steel members, such as the slenderness ratio, the axial compression ratio, the spacing ratio of diaphragms, the diameter-to-thickness ratio of the pipe-section, and the width-to-thickness ratio of the rectangular-section are considered during the parameter analysis. Eq. (1) ~ (3) are the definitions of the slenderness ratio λ, the width-thickness ratio R_R and the diameter-thickness ratio R_t, which play key roles in the design of the steel members. In the equations, r is the radius of gyration in the bending direction for the section, σ_y and σ_E are the yield stress and Euler instability stress of the steel respectively, E is the young's modulus, μ is the Poisson's ratio, and n donates the number of subpanels that the plate is divided by the longitudinal stiffeners.

$$\lambda = \sqrt{\frac{\sigma_y}{\sigma_E}} = \frac{l}{2r}\cdot\frac{1}{\pi}\sqrt{\frac{\sigma_y}{E}} \quad (1)$$

$$R_t = \frac{R}{t}\cdot\frac{\sigma_y}{E}\sqrt{3\left(1-\mu^2\right)} \quad (2)$$

$$R_R = \frac{B}{t}\sqrt{\frac{\sigma_y}{E}\frac{12\left(1-\mu^2\right)}{4n^2\pi^2}} \quad (3)$$

A total of 45 representative members are designed for analysis, including 23 pipe section members and 22 rectangular section members. The design parameters of the steel members are shown in Tables 1 and 2, in which N/N_y is the axial compression

ratio (N is the applied axial force, N_y is the squash axial force of the section), and a/R is the spacing ratio of diaphragm of the pipe section (a/R=3.5 means no diaphragms are adopted), α (=a/B) is the spacing ratio of diaphragm of the rectangular section.

Design parameters	*R*/m	*t*/m	*l*/m	R_t	λ	N/N_y	*a/R*
R_t	0.3	0.01~0.04	3.0	0.024~0.095	0.090	0.20	2.0
λ	0.3	0.02	1.5~3.5	0.047	0.045~0.105	0.20	2.0
N/N_y	0.3	0.02	3.0	0.047	0.090	0.00~0.30	2.0
a/R	0.3	0.02	3.0	0.047	0.090	0.20	1.0~3.5

Table 1: Structural design of members with pipe sections.

Design parameters	*B*/m	*t*/m	t_0/m	*l*/m	R_R	λ	N/N_y	$\alpha(=a/B)$
R_r	0.9	0.0076~0.014	0.007~0.013	5.0	0.270~0.524	0.089	0.15	0.889
λ	0.9	0.011	0.01	3.0~8.0	0.343	0.072~0.143	0.15	0.889
N/N_y	0.9	0.011	0.01	5.0	0.343	0.089	0.10~0.30	0.889
α	0.9	0.011	0.01	5.0	0.343	0.089	0.15	0.556~1.111

Table 2: Structural design of members with rectangular sections.

Numerical Technique and Theory

Figure 2 shows the numerical models created by the commercial software ABAQUS. Fixed boundaries are adopted for the member, and an axial force N and a cyclic displacement δ are applied at one end of the steel member. In order to obtain local deformation of the steel plate and the strain concentration at the welding, the shell elements are used for the numerical analysis. To facilitate the application of the load and displacement, a very short beam element is adopted at the end of the member. The beam element is connected with the shell element by MPC-beam function. The shell element model is used to analyze the steel member to obtain the load-displacement history. The most dangerous parts are re-analyzed using a more refined model, e.g. using solid elements which can simulate the details of the weld. The solid element size is less than 0.25 mm, which meets the CVGM requirement regarding to the characteristic length. The shell element model and the solid element model of the circular section member are divided into about 25,000 and 45,000 elements respectively, and the plate and shell element model and the solid element model of the rectangular section member are both divided into about 35,000 elements. The shell element model and the solid element model of the pipe section member are divided into about 25,000 and 45,000 elements, respectively. The shell element model and the solid element model of the rectangular section member are both divided into about 35,000 elements.

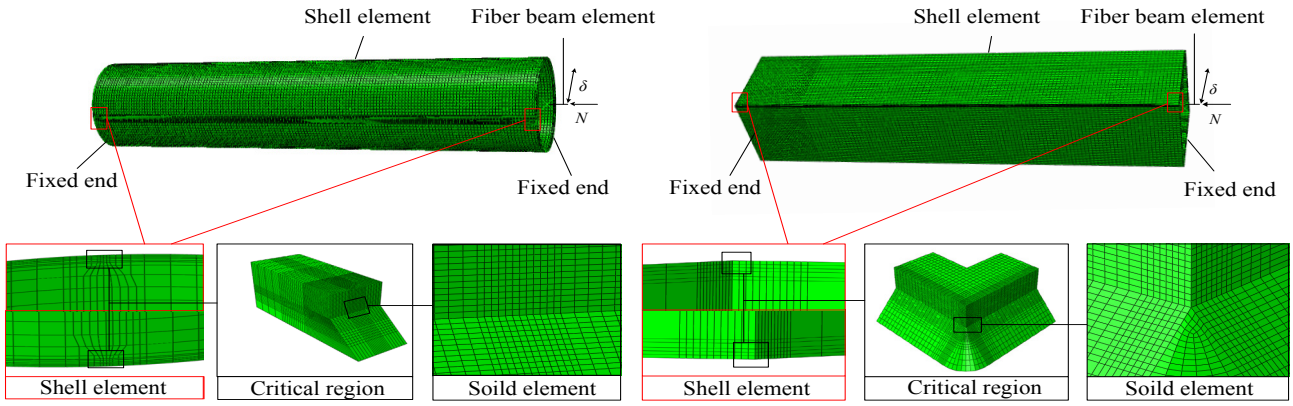

Figure 2: Numerical model and element division of the member.

Ultralow cycle fatigue is composed of the micro-void nucleation, dilation, contraction and coalescence. Due to the different effects of tension and compression, the index VGI_{cyclic} is defined as [15-19]:

$$VGI_{cyclic} = \sum_{\text{tensile-cycles}} \int_{\varepsilon_1}^{\varepsilon_2} \exp\left(\left|1.5T\right|\right) \mathrm{d}\varepsilon_{eq}^{p} - \sum_{\text{compressive-cycles}} \int_{\varepsilon_1}^{\varepsilon_2} \exp\left(\left|1.5T\right|\right) \mathrm{d}\varepsilon_{eq}^{p} \quad (4)$$

where T is the stress triaxiality. According to the calibration of the circular specimen test, an exponential decay function is selected to express the critical void growth parameter $\mathrm{VGI}_{\mathrm{cyclic}}^{\mathrm{critical}}$ for cyclic loading:

$$VGI_{cyclic}^{critical} = \eta \exp\left(-\lambda_{CVGM}\varepsilon_{eq}^{p}\right) \quad (5)$$

where λ_{CVGM} is a material-dependent damageability coefficient, the cumulative equivalent plastic strain $\varepsilon_{\mathrm{eq}}^{\mathrm{p}}$ is calculated at the beginning of each tensile excursion, and η is the toughness parameter related to the material property. ULCF fracture is thought to occur when $\mathrm{VGI}_{\mathrm{cyclic}}$ exceeds its critical value $\mathrm{VGI}_{\mathrm{cyclic}}^{\mathrm{critical}}$. In order to illustrate the development process of ULCF damage, the damage index D of the CVGM is defined in this study. D=0 means no fatigue damage, while D=1.0 indicates ULCF crack occurs.

$$D = \frac{VGI_{cyclic}}{VGI_{cyclic}^{critical}} \quad (6)$$

A UVARM subroutine is coded using FORTRAN language to implement CVGM to the ABAQUS software. Since CVGM parameter calibration is based on the Chaboche combined hardening model [22,29], the hardening model is also used herein. Table 3 shows the mechanical parameters of Q345 steel [29], where $\sigma|_0$ is the initial yielding strength, Q_∞ is the maximum hardening value of the yield surface, and b is the rate of change in yield surface to the development of plastic strain. C_k is the initial modulus of the kinematic hardening, and γ_k is the ratio of the kinematic hardening module ratio to the plastic strain.

Material	$\sigma\|_0$(MPa)	Q_∞(MPa)	b	C_1(MPa)	γ_1	C_2(MPa)	γ_2	C_3(MPa)	γ_3
Base Metal (BM)	354.10	13.2	0.6	44373.7	523.8	9346.6	120.2	946.1	18.7
Heat-Affected Zone (HAZ)	312.57	9.8	0.7	32242.4	199.2	3858.5	43.1	329.2	0.3
Weld Metal (WM)	428.45	17.4	0.4	12752.3	160.0	1111.2	160.0	630.5	26.0

Table 3: Parameters in combined hardening model for Q345 steel.

The applied cyclic displacement δ is shown in Figure 3, in which δ_y is the yield displacement corresponding to the yield thrust H_y of the member. The member is subjected to a cyclic displacement with increasing amplitudes which repeats for 3 loops.

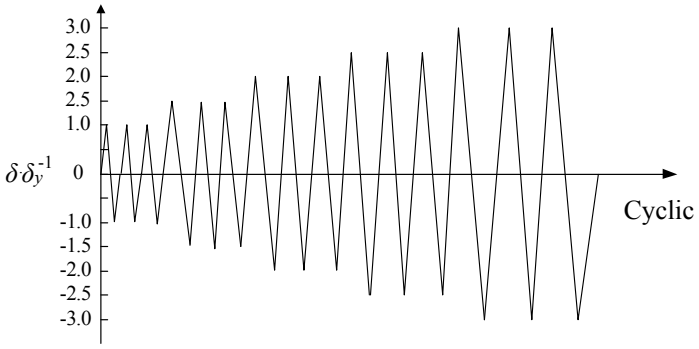

Figure 3: Cyclic loading method.

Analysis of ULCF Damage Index

Different ultimate states are adopted to represent the instability state and failure. The load-displacement curve and its envelope of the member are obtained through numerical analysis. The ULCF damage indexes D at the most dangerous areas are obtained corresponding to the bearing capacity state [13], the state where the strength reaches the peak value and decreased to 95% of the peak value [4,7], and the state where the strength decreased to 90% of the peak value [30], respectively. Through analyzing the index value D corresponding to these critical states, the relationship between the instability failure mode and the ULCF failure mode can be determined.

ULCF damage under critical states

Figure 4 shows the local deformation of the steel plate of the member in the bearing capacity state. Local buckling can be observed at the boundary of the members, thus the most dangerous position of the member can be determined where ULCF may occur. These critical areas, including the welding, heat-affected zone and base metal are re-analyzed using solid element models.

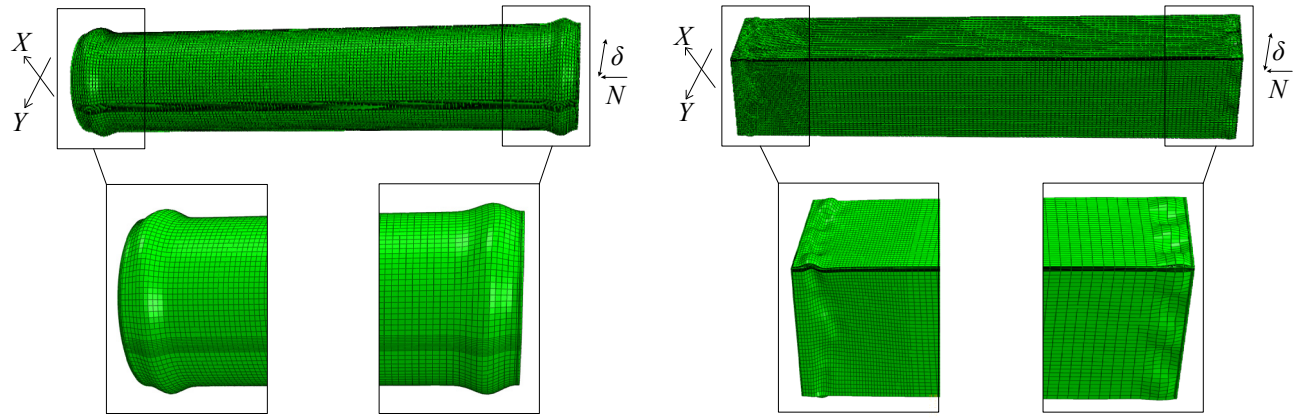

Figure 4: Local buckling and deformation of the member.

Figure 5 shows the ULCF damage index D of pipe cross-section members corresponding to the predefined ultimate states, where H_m is the peak strength on the envelope curve. $1.00H_m$, $0.95H_m$ and $0.90H_m$ in the figure represent the defined critical states, respectively. D_W, D_H and D_B represent the ULCF damage indexes of the weld zone, the heat-affected zone and the base metal, respectively. The results show that the damage index increases during the loading process. If the axial compression ratio $N/N_y \geq 0.2$, or the slenderness ratio $\lambda \geq 0.06$, or the diameter-to-thickness ratio $R_t \geq 0.05$, the ultralow cycle fatigue damage index is less than 1.0, which indicates the member experiences instability failure; if $R_t < 0.03$, fatigue crack occurs at both the heat-affected zone and the weld zone prior to structural instability. When the structural strength decreases to $0.95H_m$ and $0.90H_m$, the ULCF damage is greatly affected by the axial compression ratio, slenderness ratio and diameter-to-thickness ratio. The spacing ratio of diaphragm has marginal effect on the fatigue damage. Moreover, the heat-affected zone and weld zone are more vulnerable to ultralow cycle fatigue than the base metal.

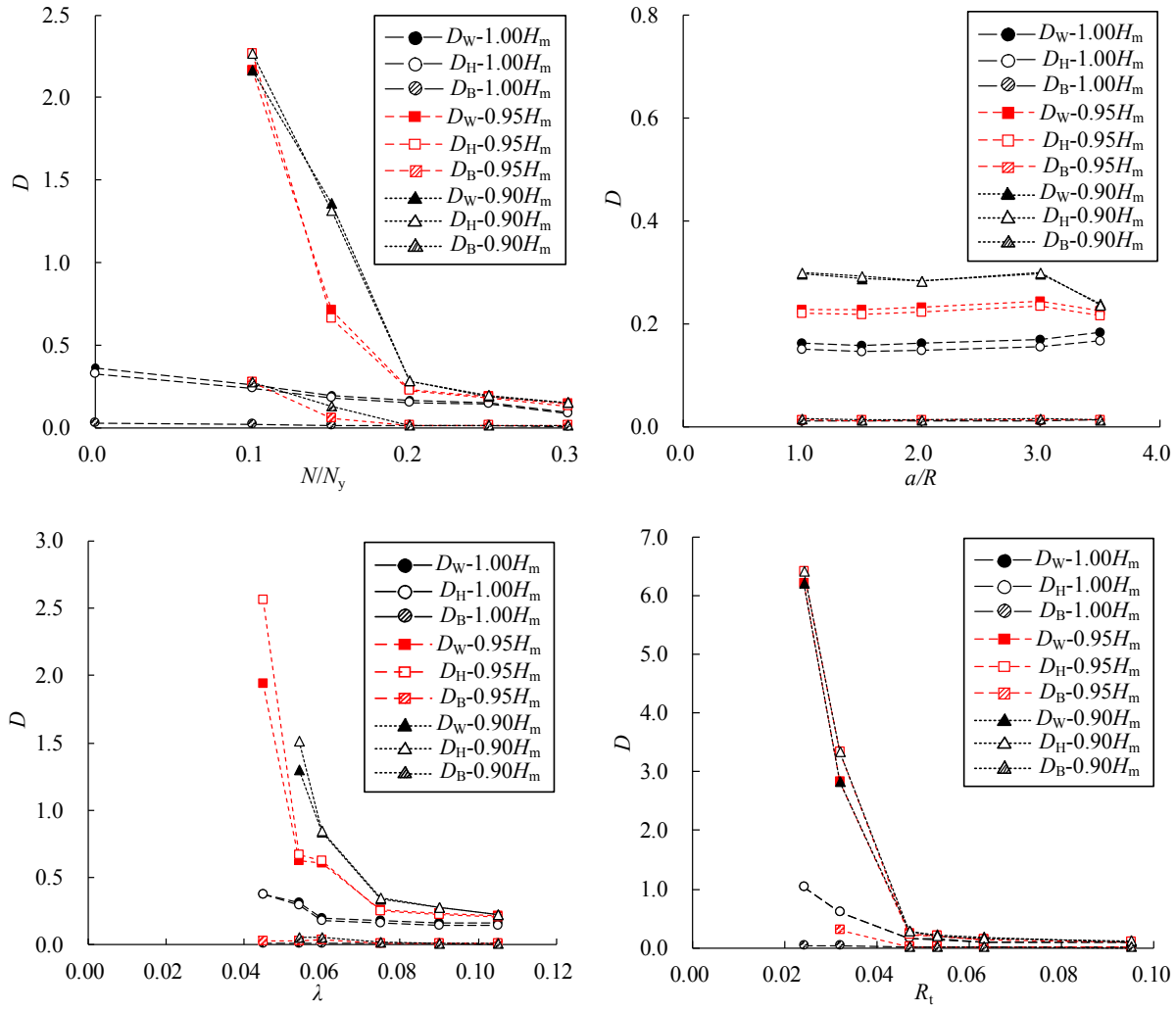

Figure 5: ULCF damage index of pipe-section members.

Figure 6 shows the ULCF damage index D of rectangular cross-section members. The results show that when the structural strength reaches the peak value, fatigue damage indexes of the welding and heat-affected zone are significantly greater than 1.0, indicating that the members experience ULCF failure rather than the instability failure. The design parameters have a great influence on the ultralow cycle fatigue damage index of the welding and the heat-affected zone of the rectangular section. In addition, the damage index of heat-affected zone is greater than that of weld zone and base material, and the heat-affected zone is more prone to ultralow cycle fatigue.

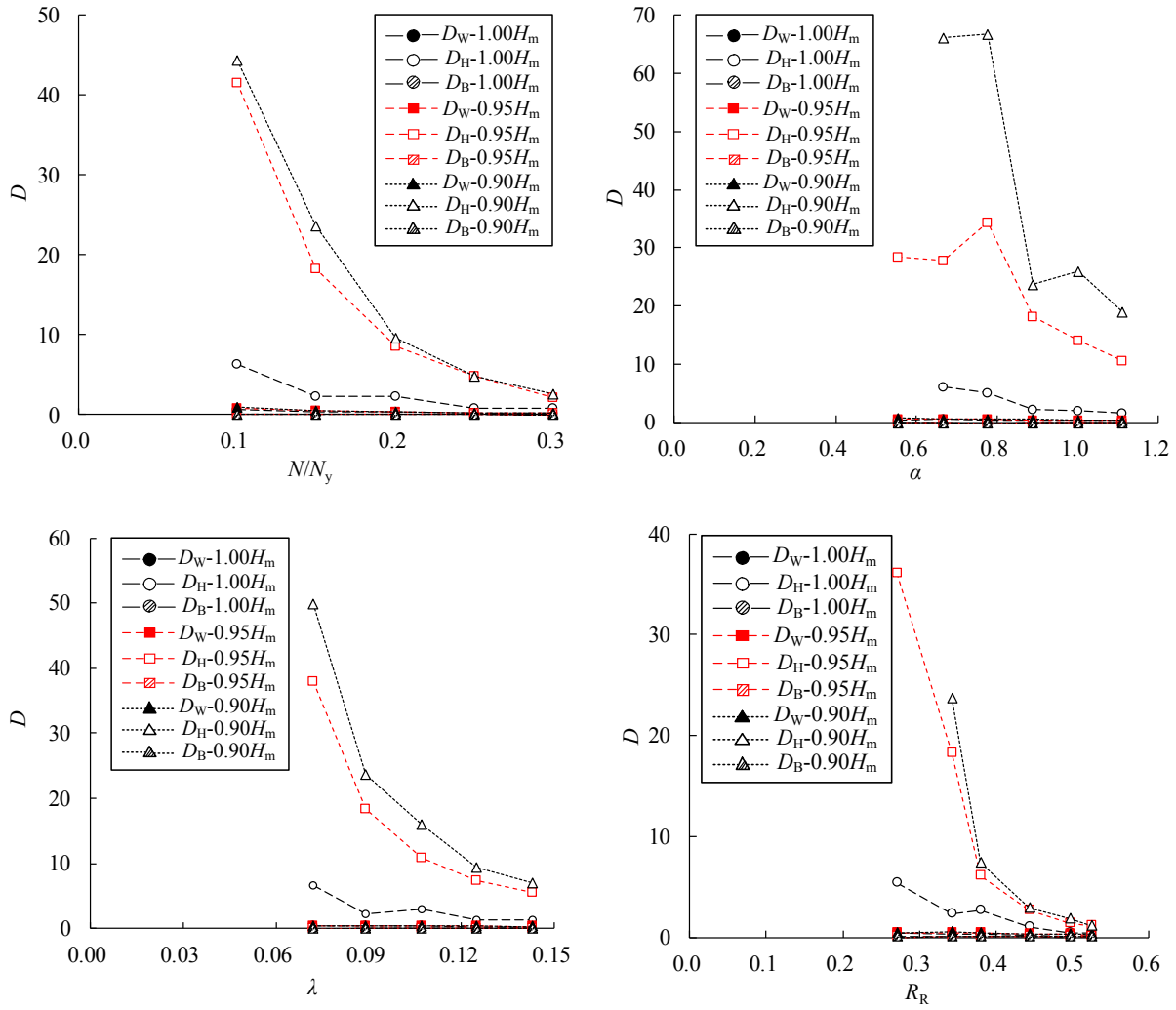

Figure 6: ULCF damage index of rectangular-section members.

Evaluation of ultralow cycle fatigue damage

In order to facilitate the prediction of the failure mode of the member, the ULCF damage values of the welding, the heat-affected zone and the base metal under different critical states are fitted and analyzed. Thus, some empirical prediction formulas are proposed. Figure 7 shows the fitting results of the ULCF index. The axial compression ratio, slenderness ratio and diameter-thickness ratio are considered for the pipe-section members, while the axial compression, the spacing ratio of diaphragm, slenderness ratio and width-thickness ratio are considered for the rectangular-section members. The results show that the ULCF index can be predicted accurately, and the determination coefficients of all fitting curves are greater than 0.8. These prediction formulas can be used for seismic design of steel members and avoid great efforts conducting the complicated numerical analysis.

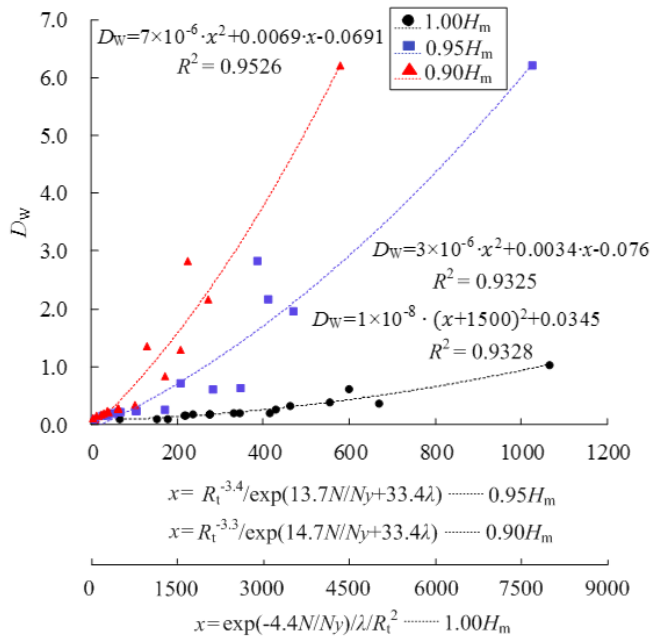

(a) Welding in pipe-section members

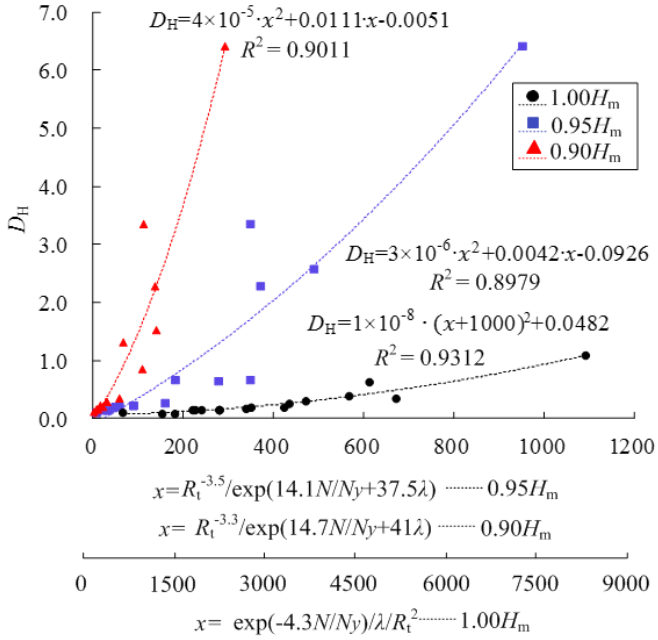

(b) Heat-affected zone in pipe-section members

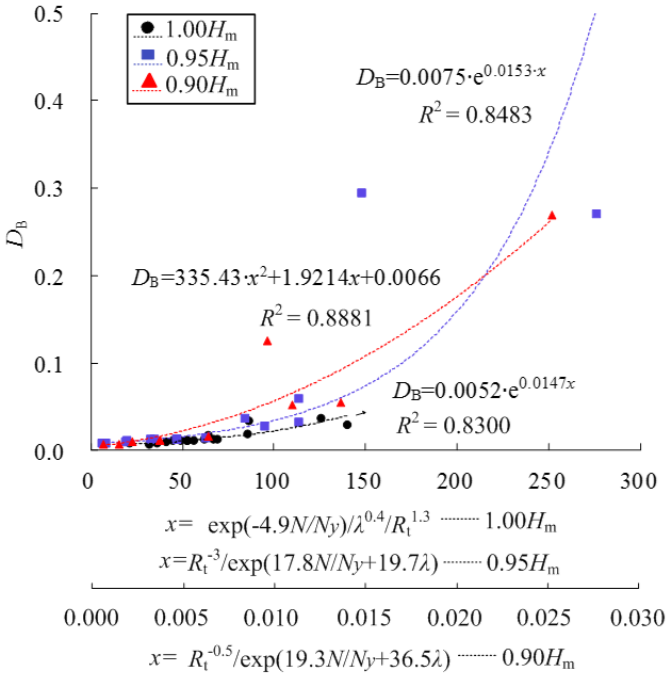

(c) Base metal in pipe-section members

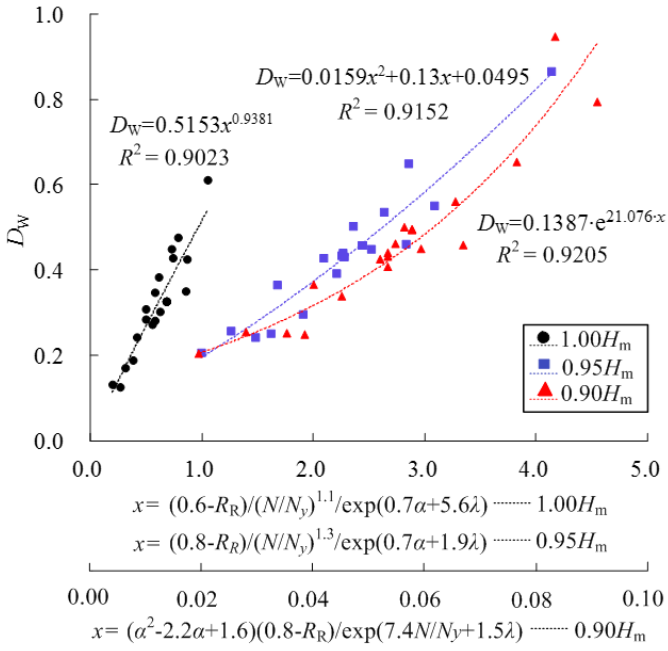

(d) Welding in rectangular-section members

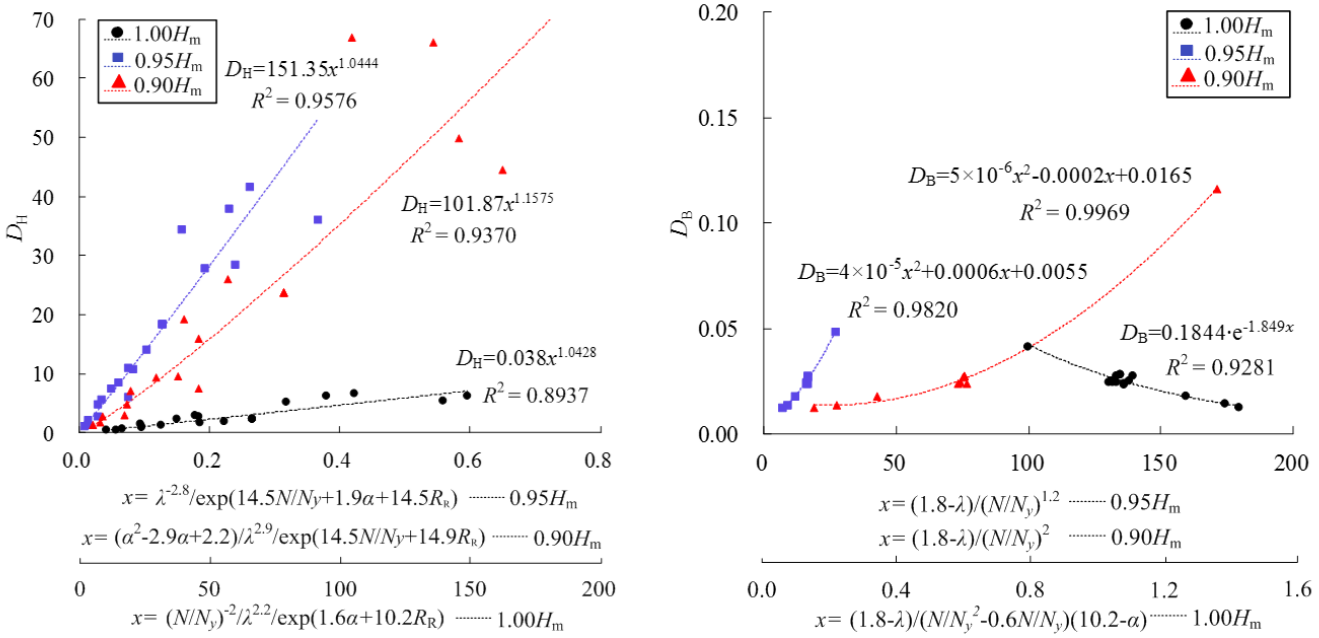

(e) Heat-affected zone in rectangular-section members (f) Base metal in rectangular-section members

Figure 7: Fitting curves of ULCF damage index.

Eq. (7) ～ (9) are the ULCF damage indices fitting formulas for the pipe-section members:

$$1.00H_m\begin{cases} D_W=1\times10^{-8}\cdot\left[\exp\left(-4.4N/N_y\right)/\lambda/R_t^2+1500\right]^2+0.0345 \\ D_H=1\times10^{-8}\cdot\left[\exp\left(-4.3N/N_y\right)/\lambda/R_t^2+1000\right]^2+0.0482 \\ D_B=0.0052\cdot\exp\left[0.0147\cdot\exp\left(-4.9N/N_y\right)/\lambda^{0.4}/R_t^{1.3}\right] \end{cases} \quad (7)$$

$$0.95H_m\begin{cases} D_W=3\times10^{-6}\cdot\left[R_t^{-3.4}/\exp\left(13.7N/N_y+33.4\lambda\right)+566.7\right]^2-0.8873 \\ D_H=3\times10^{-6}\cdot\left[R_t^{-3.5}/\exp\left(14.1N/N_y+37.5\lambda\right)+700\right]^2-1.56 \\ D_B=0.0075\cdot\exp\left\{0.0153\cdot\exp\left[R_t^{-3}/\exp\left(17.8N/N_y+4.5\lambda\right)\right]\right\} \end{cases} \quad (8)$$

$$0.90H_m\begin{cases} D_W=7\times10^{-6}\cdot\left[R_t^{-3.3}/\exp\left(14.7N/N_y+7.6\lambda\right)+492.86\right]^2-1.769 \\ D_H=4\times10^{-5}\cdot\left[R_t^{-3.3}/\exp(14.7N/N_y+41\lambda)+138.75\right]^2-0.775 \\ D_B=335.43\cdot\left[R_t^{-0.5}/\exp\left(19.3N/N_y+36.5\lambda\right)+0.0028\right]^2+0.0038 \end{cases} \quad (9)$$

Eq. (10) ～ (12) are the fitting formulas for the rectangular-section members:

$$1.00H_m\begin{cases} D_W=0.5153\cdot\left[(0.6-R_R)/(N/N_y)^{1.1}/\exp(0.7\alpha+5.6\lambda)\right]^{0.9381} \\ D_H=0.038\cdot\left[(N/N_y)^{-2}/\lambda^{2.2}/\exp(1.6\alpha+10.2R_R)\right]^{1.0428} \\ D_B=0.1844\cdot\exp\left[-1.849\cdot(1.8-\lambda)/(N/N_y{}^2-0.6N/Ny)(10.2-\alpha)\right] \end{cases} \quad (10)$$

$$0.95H_m\begin{cases} D_W=0.0159\cdot\left[(0.8-R_R)/(N/N_y)^{1.3}/\exp(0.7\alpha+1.9\lambda)+4.09\right]^2-0.2162 \\ D_H=151.35\cdot\left[\lambda^{-2.8}/\exp(14.5N/N_y+1.9\alpha+14.5R_R)\right]^{1.0444} \\ D_B=4\times10^{-5}\cdot\left[(1.8-\lambda)/(N/N_y)^{1.2}+7.5\right]^2 \end{cases} \quad (11)$$

$$0.90H_m\begin{cases} D_W=0.1387\cdot\exp\left[21.076\cdot(\alpha^2-2.2\alpha+1.6)(0.8-R_R)/\exp(7.4N/N_y+1.5\lambda)\right] \\ D_H=101.87\cdot\left[(\alpha^2-2.9\alpha+2.2)/\lambda^{2.9}/\exp(14.5N/N_y+14.9R_R)\right]^{1.1575} \\ D_B=5\times10^{-6}\cdot\left[(1.8-\lambda)/(N/N_y)^2-20\right]^2-0.0145 \end{cases} \quad (12)$$

Conclusions

The failure mode of fixed steel members under cyclic loads were analyzed in this paper, and the influences of design parameters on the ultralow cycle fatigue damage under different critical instable states were discussed. Empirical formulas for predicting ultralow cycle fatigue damage of steel members were proposed. Some conclusions can be drawn as follows:

1. As the cyclic loading proceeds, the ultralow cycle fatigue damage of the steel member increases gradually. The ultralow cycle fatigue damage index of the heat-affected zone is obviously greater than that of the weld zone and the base metal, indicating the heat-affected zone is more vulnerable to ultralow cycle fatigue damage.
2. For the pipe-section steel member, if the axial compression ratio is greater than 0.2, or the slenderness ratio is greater than 0.06, or the diameter-to-thickness ratio is greater than 0.05, the member can experience instability failure under cyclic loads, which is prior to ULCF failure. If the diameter-to-thickness ratio is less than 0.03, the ultralow cycle fatigue failure occurs prior to structural instability. The ultralow cycle fatigue damage index at the critical state is greatly affected by the axial compression ratio, slenderness ratio and diameter-to-thickness ratio, but is less affected by the spacing ratio of diaphragms.
3. For the rectangular-section steel members, if the width-to-thickness ratio is greater than 0.5, the instability failure controls the safety of the members under strong earthquakes. If the width-to-thickness ratio is less than 0.5, the members are prone to failure due to ultralow cycle fatigue.
4. The prediction formulas of the ultralow cycle fatigue damage are proposed, which can avoid a very high computational cost conducting ultralow cycle fatigue analysis, and they are very useful for preliminary seismic design of the steel members.

Acknowledgments

The research work described in this paper was financially supported by the grants from the National Natural Science Foundation of China (No. 51708485), the Jiangsu Planned Projects for Postdoctoral Research Funds (No. 1701191B), and the China Postdoctoral Science Foundation (No. 2017M611925). Their support is gratefully acknowledged by the authors.

References

1. Watanabe E, Sugiura K, Nagata K, Kitane Y (1998) Performances and damages to steel structures during the 1995 Hyogoken-Nanbu earthquake. Engineering Structures 20: 282-290.
2. Usami T (1996) Interim guidelines and new technologies for seismic design of steel structures. Tokyo: Committee on New Technology for Steel Structures (CNTSS), JSCE.
3. Liang JJ, Ge HB (2019) Ultra-low-cycle fatigue failure of metal structures under strong earthquakes. Singapore: Springer Nature Singapore Pte Ltd.
4. Zheng Y, Usami T, Ge HB (2000) Ductility of thin-walled steel box stub-columns. Journal of Structural Engineering 126: 1304-1311.

5. Kono T, Ge HB, Usami T (2003) Re-examination of the ultimate strain formula for steel box stub-columns and its application in steel arch bridges. Proceedings of the 6th Symposium on Ductility Design Method for Bridges, Ductility Design Subcommittee, Tokyo. 323-328.

6. Ge HB, Gao SB, Usami T (2000) Stiffened steel box columns. Part 1: cyclic behavior. Earthquake Engineering and Structural. Dynamics 29: 1691-1706.

7. Usami T, Ge HB, Gao SB (2000) Stiffened steel box columns. Part 2: ductility evaluation. Earthquake Engineering and Structural. Dynamics 29: 1707-1722.

8. Ge HB, Gao SB, Usami T (1997) Numerical study on cyclic elasto-plastic behavior of steel bridge piers of pipe-sections without stiffeners. Journal of JSCE 577: 181-190. (In Japanese).

9. Usami T, Fukumoto Y (1982) Local and Overall Buckling of Welded Box Columns. Journal of the Structural Division 108: 525-543.

10. Zhou SP, Chen WF (1985) Design criteria for box columns under biaxial loading. Journal of Structural Engineering 111: 2643-2659.

11. GB 50017-2017 (2017) Code for design of steel structure. Beijing: China Architecture & Building Press. (In Chinese).

12. JTG D64-2015 MOT (2015) Specifications for Design of highway steel bridge. Beijing: China Communications Press. (In Chinese).

13. Japanese Road Association (2012) Specifications for highway bridges, Part V: Seismic design. Tokyo: Maruzen.

14. AASHTO (2011) Guide specifications for LRFD seismic bridge design. Washington DC: American Association of State Highway and Transportation Officials, 2nd edition.

15. Rice JR, Tracey DM (1969) On the ductile enlargement of voids in triaxial stress fields. Journal of the Mechanics and Physics of Solids 17: 201-217.

16. Kanvinde AM, Deierlein GG (2006) Void growth model and stress modified critical strain model to predict ductile fracture in structural steels. Journal of Structural Engineering 132: 1907-1918.

17. Kanvinde AM, Deierlein GG (2007) Finite-element simulation of ductile fracture in reduced section pull-plates using micromechanics-based fracture models. Journal of Structural Engineering 133: 656-664.

18. Kanvinde AM, Deierlein GG (2007) Cyclic void growth model to assess ductile fracture initiation in structural steels due to ultra-low cycle fatigue. Journal of Engineering Mechanics, ASCE 133: 701-712.

19. Kanvinde AM, Gomez IR, Roberts M, Fell BV, Grondin GY (2009) Strength and ductility of fillet welds with transverse root notch. Journal of Constructional Steel Research 65: 948-958.

20. Liao FF, Wang W, Chen Y (2012) Parameter calibrations and application of micromechanical fracture models of structural steels. Structural Engineering and Mechanics 42: 153-174.

21. Liao FF, Wang MQ, Tu LS, Wang J, Lu L (2019) Micromechanical fracture model parameter influencing factor study of structural steels and welding materials. Construction and Building Materials 215: 898-917.

22. Yin Y, Li S, Han Q, Lei P (2019) Calibration and verification of cyclic void growth model for 20Mn5QT cast steel. Engineering Fracture Mechanics 206: 310-329.

23. Zhou H, Wang Y, Yang L, Shi Y (2014) Seismic low-cycle fatigue evaluation of welded beam-to-column connections in steel moment frames through global-local analysis. International Journal of Fatigue 64: 97-113.

24. Zhou H, Wang Y, Shi Y, Xiong J, Yang L (2013) Extremely low cycle fatigue prediction of steel beam-to-column connection by using a micro-mechanics based fracture model. International Journal of Fatigue 48: 90-100.

25. Wang Y, Zhou H, Shi Y, Chen C (2010) Fracture behavior analyses of welded beam-to-column connections based on elastic and inelastic fracture mechanics. International Journal of Steel Structures 10: 253-265.

26. Xie X, Zhuge HQ, Tang ZZ, Wang T, Liao Y (2018) Damage characteristics of thin-walled steel arch bridges subjected to in-plane earthquake action. Journal of Constructional Steel Research 151: 70-82.

27. Kuwamura H, Yamamoto K (1997) Ductile crack as trigger of brittle fracture in steel. Journal of Structural Engineering 123: 729-735.

28. Chen WF, Duan L (2014) Bridge engineering handbook. Second edition: Seismic design, CRC Press.

29. Liao YH (2018) Research on ultra-low cycle fatigue properties and fracture mechanism of steel bridge welded joint. Master's Thesis, Zhejiang University, Hangzhou, China. (In Chinese).

30. Yamada S, Jiao Y, Narihara H, Yasuda S, Hasegawa T (2014) Plastic deformation capacity of steel beam-to-column connection under long-duration earthquake. International Journal of High-Rise Buildings 3: 231-241.